Hamburger Beiträge
zur Angewandten Mathematik

On the Simulation of Cavitation in Hydraulic Pipelines based on the Thermodynamic and Caloric Properties of Liquid and Steam

U. Iben, A. Berg, A. Meister, J. Schmidt

Reihe F
Computational Fluid Dynamics and Data Analysis 16
October 2001

Hamburger Beiträge zur Angewandten Mathematik

Reihe A	Preprints
Reihe B	Berichte
Reihe C	Mathematische Modelle und Simulation
Reihe D	Elektrische Netzwerke und Bauelemente
Reihe E	Scientific Computing
Reihe F	Computational Fluid Dynamics and Data Analysis

On the Simulation of Cavitation in Hydraulic Pipelines based on the Thermodynamic and Caloric Properties of Liquid and Steam.

U. Iben*, A. Berg*, A. Meister†, J. Schmidt‡

October 23, 2001

Abstract

The simulation of cavitation phenomena plays an important role for the development of modern hydraulic tools and injection systems. Cavitation leads to a reduction of mass flow and influences the wave motion in hydraulic components significantly. The article deals with the simulation of a homogeneous cavitation model based on the thermodynamic and caloric properties of liquid and steam with the goal to study basic physical phenomena and time dependent properties. The presented model and numercial scheme can be applied to the simulation of more complex hydraulic systems.

1 Introduction

The necessity to simulate cavitated flows arises from the demand to prevent damages and to understand the dynamic properties in the early development phase of hydraulic tools. Fast working valves, strongly time depending high and low pressure levels, and a large range of temperature can lead to evaporation of oil in hydraulic pipelines and valves. The evaporation leads to a significant reduction of the speed of sound in the mixture, reduces the mass flow, and therefore influences the working properties of the valves. Condensation of vapor bubbles can lead to noise and damages in the hydraulic components. In order to describe the complex time dependent physical processes and protect technical tools of cavitation erosion, numerical simulations prove to be very helpful.
Many papers deal with this topic, see for example [9, 11, 17, 20]. In general, a combination of continuous and discrete models is used. The flow is described with the Euler or the Navier-Stokes equations, representing the continuous model, whereas the cavitation is modeled by discrete bubble models where oscillations of single bubbles or bubble clouds are considered, cf. [3, 17, 19, 20]. These models include many unknown physical values and properties, such as the bubble diameter, the bubble number density, and the extreme complicated bubble interactions. Due to this reason, these models are difficult to handle for real industrial applications. The experimental and numerical study of single phenomena using these models are time consuming too. Single bubble phenomena, such as the collapsing of bubbles are investigated by experiments and numerical studies by Ohl and Ory, [18]. For bubble clouds and interaction of bubbles, experimental studies were published in [6].
Pioneering works of one-dimensional two phase flow were published by Wallis [23] and Kolev [15]. Cavitated flow can be described by several models with different model levels. A first approach could be to start with the conservation equations of the homogeneous mixture as done in [4, 9]. In this case the evaporation and condensation process is described by the equation of state, i.e.

*Robert Bosch GmbH, Dept. FV/FLM, P.Box 106050, D-70059 Stuttgart
†Department of Mathematics, University of Hamburg, Bundesstrasse 55, D-20146 Hamburg
‡Institute for Fluid Dynamics and Thermodynamics, Otto-von-Guericke-University Magdeburg, D-39106 Magdeburg

$\rho = \rho(p, T = fixed)$. This approach can lead to stability problems due to the large range of the mixture density and propagation speed. In Beck [4] a combination of an explicit and locally implicit scheme is used successfully to avoid these stability problems. As a next step one will split the continuity equation for the gas and liquid phase and couple it by a source term as done in [25] for isotropic water flow, i.e. the equation describing the conservation of energy was neglected. It can be shown analytically, that this approach is equivalent to the approach using the mixture equations only, cf. [14]. Currently the last step following this approach consists in introducing the energy equation for the homogeneous mixture in connection with thermodynamic equilibrium or non-equlibrium models for the phase transition and an additional heat flux to the system. In this paper we will follow this last approach to describe cavitational effects in one space dimension in a pipe.
Throughout the paper we shall make use of the following notation: The index G denotes the gas and steam phase, the index L denotes the liquid phase. Physical values denoting a mixture are written without an index.

2 Modeling of the System of Equations

Every fluid contains unsolved and solved air. Speaking about cavitation we need to distinguish between gas-cavitation and "real" cavitation. The so-called gas cavitation constitutes a diffusion process which we will not discuss in this context. We assume that the fluid contains a fixed mass-fraction of unsolved air as a homogeneous gas-liquid mixture which influences the fluid properties, especially the speed of sound of the liquid-gas mixture. In particular for small pressure values this decrease becomes apparent, cf. [14, 23]. The strong dependence of the speed of sound on the unsolved air and steam leads to the fact, that the wave motion appears to be a discontinuous and nonlinear process.
As the velocities of fluid v_L and gas/steam v_G in a pipe are approximately the same, a homogeneous mixture is considered, i.e. $v_L = v_G = v$. This assumption makes sense for acoustic cavitation and low speeds of the mixture. The cavitation provoked by pressure waves appears as small bubbles or steam clouds. In order to apply a numerical scheme we assume the steam to be equally distributed within the computational cells. Note, that due to the wave motion in a pipe, the fluid can not evaporate completely. For a complete evaporation, an additional heat flux to the mixture is necessary. For this reason, the mass fraction as well as the volume fraction of the steam are always smaller than one. The mass fraction μ and the volume fraction ε are defined by

$$\mu = \frac{m_{\mathrm{G}}}{m} \quad \text{and} \quad \varepsilon = \frac{V_{\mathrm{G}}}{V}.$$

Therefore the mixture density is given by

$$\rho = \varepsilon\rho_{\mathrm{G}} + (1-\varepsilon)\rho_{\mathrm{L}} \quad \text{or} \quad \frac{1}{\rho} = \frac{\mu}{\rho_{\mathrm{G}}} + \frac{1-\mu}{\rho_{\mathrm{L}}}. \tag{2.1}$$

By following the described approach of splitting the continuity equation and coupling the resulting equations by a source term, but leaving the momentum and energy equation untouched we get the two phase Euler equations in one space dimension (for a more detailed derivation of the system confer to [14, 25]):

$$\begin{aligned}
\frac{\partial}{\partial t}(\varepsilon\rho_{\mathrm{G}}) + \frac{\partial}{\partial z}(\varepsilon\rho_{\mathrm{G}} v) &= \Gamma, \\
\frac{\partial}{\partial t}\left((1-\varepsilon)\rho_{\mathrm{L}}\right) + \frac{\partial}{\partial z}\left((1-\varepsilon)\rho_{\mathrm{L}} v\right) &= -\Gamma, \\
\frac{\partial}{\partial t}(\rho v) + \frac{\partial}{\partial z}(\rho v^2 + p) &= 0, \\
\frac{\partial}{\partial t}\left(\rho(e + v^2/2)\right) + \frac{\partial}{\partial z}\left(\rho v(e + v^2/2 + p/\rho)\right) &= 0.
\end{aligned} \tag{2.2}$$

As mentioned earlier the source term Γ describes the evaporation and condensation process of cavitation. The inner energy e is connected with the enthalpy h by

$$h = e + \frac{p}{\rho}.$$

We assume the gas/steam and liquid phase to have the same temperature T. This represents a first useful assumption for the presented model. As known by experiments, a fast compression of the gas-liquid mixture to a very high pressure level leads to an adiabatic compression of the air bubbles in the fluid. Thus, the temperature inside the air bubbles grows significantly. In order to consider such effects, energy equations for both phases have to be considered separately and a source term containing all these effects needs to be derived. Obviously we chose to neglect all of these and related effects, but consider only one energy equation for the mixture.
Following [16], the number of partial-differential equations used in existing one-dimensional models varies between 3 conservation equations for the mixture and 6 conservation equations for each phase separately. The splitting in (2.2) was chosen to avoid stability problems using the homogeneous mixture model and can also be used for non-equilibrium models derived in [13, 14, 1].
The pressure p is a function of the density and the temperature which is given implicitly only. This reveals a main difference to the modeling of problems in gas dynamics. A system of nonlinear equations has to be solved in each time step in order to compute the primitive variables p, T and ε from the conservative variables

$$u_1 = \varepsilon\rho_{\mathrm{G}}, \quad u_2 = (1-\varepsilon)\rho_{\mathrm{L}}, \quad u_3 = \rho v \quad \text{and} \quad u_4 = \rho\left(e + \frac{v^2}{2}\right)$$

which are used to solve the system (2.2) numerically.
The modeling of the source term Γ is not easy to derive, see [8, 14, 25]. If we consider just the gaseous phase in a one-dimensional flow, the mass conservation law can be written as follows:

$$\frac{\partial}{\partial t}(\varepsilon\rho_{\mathrm{G}}) + \frac{\partial}{\partial z}(\varepsilon\rho_{\mathrm{G}} v) = \rho\frac{\mathrm{d}\mu}{\mathrm{d}t} = \Gamma. \tag{2.3}$$

Note, that the mass exchange on the right hand side of eq.(2.3) must be the substantial derivative of the gaseous mass because the mass exchange is strongly coupled to the fluid elements. A similar procedure leads to the continuity equation for the liquid phase

$$\frac{\partial}{\partial t}((1-\varepsilon)\rho_{\mathrm{L}}) + \frac{\partial}{\partial x}((1-\varepsilon)\rho_{\mathrm{L}} v) = -\rho\frac{\mathrm{d}\mu}{\mathrm{d}t}. \tag{2.4}$$

Note, that summation of eq. (2.3) and (2.4) holds the continuity equation for the mixture. The system of conservation equations (2.2) will be abbreviated by

$$\frac{\partial}{\partial t}\mathbf{u} + \frac{\partial}{\partial z}\mathbf{f}(\mathbf{u}) = \mathbf{g}(\mathbf{u}) \quad \text{with} \quad \mathbf{u} = (u_1, u_2, u_3, u_4)^T. \tag{2.5}$$

In order to use numerical schemes of high accuracy, the Jacobian of the flux vector $\mathbf{f}$ has to be computed. Following [14, 5], the four eigenvalues are:

$$\lambda_1 = v - c, \quad \lambda_2 = \lambda_3 = v, \quad \text{and} \quad \lambda_4 = v + c \tag{2.6}$$

where c is the speed of sound for the homogeneous mixture. The eigenvalues λ_1 and λ_4 represent the characteristics of the system (2.2), while the eigenvalues $\lambda_2 = \lambda_3$ represent the path. For fixed mass fraction μ the speed of sound c in the mixture can be computed as a function of the volume fraction ε and the speeds of sound and densities of each component by

$$\frac{1}{\rho c^2} = \frac{\varepsilon}{\rho_G c_G^2} + \frac{(1-\varepsilon)}{\rho_L c_L^2}. \tag{2.7}$$

Equation (2.7) was conducted by Wallis in the first place, cf. [23]. It can be derived by different ways, see [23] and [14]. To solve (2.2) numerically, the first order HLL-scheme in connection with operator splitting is used, cf. [21]. The computational domain $[0, 0.1] \times [0, T]$ is spatially equidistant spaced, i.e.

$$0 = z_0 < z_1 < \cdots < z_i < \cdots z_{N-1} < z_N = 0.1, \quad \text{with} \quad \Delta z := z_{i+1} - z_i = \text{const.}$$

Regarding the domain of time, we get

$$0 = t^0 < t^1 < \cdots < t^n < \cdots \leq t_{end} \quad \text{with} \quad \Delta t = t^{n+1} - t^n,$$

and Δt depending on the propagation speeds, cf. (2.11). Furthermore we introduce the notation

$$\mathbf{u}_i^n = \begin{pmatrix} u_{1,i}^n \\ u_{2,i}^n \\ u_{3,i}^n \\ u_{4,i}^n \end{pmatrix} \quad \text{with} \quad u_{k,i}^n = u_k(z_i, t^n),\ k = 1, 2, 3, 4.$$

According to E.F.Toro in [21], the discretization of a homogeneous hyperbolic equation using the HLL-scheme can be written in the following form:

$$\mathbf{u}_i^{n+1} = \mathbf{u}_i^n + \frac{\Delta t}{\Delta z}\left(\mathbf{F}_{i-1/2}^{\mathrm{HLL}} - \mathbf{F}_{i+1/2}^{\mathrm{HLL}}\right), \tag{2.8}$$

with numerical flux vectors $\mathbf{F}^{\mathrm{HLL}}$ defined by

$$\mathbf{F}_{i+\frac{1}{2}}^{\mathrm{HLL}} = \frac{a_{\mathrm{R},i+1}^n \mathbf{f}(\mathbf{u}_i^n) - a_{\mathrm{L},i}^n \mathbf{f}(\mathbf{u}_{i+1}^n) + a_{\mathrm{L},i}^n a_{\mathrm{R},i+1}^n (\mathbf{u}_{i+1}^n - \mathbf{u}_i^n)}{a_{\mathrm{R},i+1}^n - a_{\mathrm{L},i}^n} \tag{2.9}$$

$$\mathbf{F}_{i-\frac{1}{2}}^{\mathrm{HLL}} = \frac{a_{\mathrm{R},i}^n \mathbf{f}(\mathbf{u}_{i-1}^n) - a_{\mathrm{L},i-1}^n \mathbf{f}(\mathbf{u}_i^n) + a_{\mathrm{L},i-1}^n a_{\mathrm{R},i}^n (\mathbf{u}_i^n - \mathbf{u}_{i-1}^n)}{a_{\mathrm{R},i}^n - a_{\mathrm{L},i-1}^n}. \tag{2.10}$$

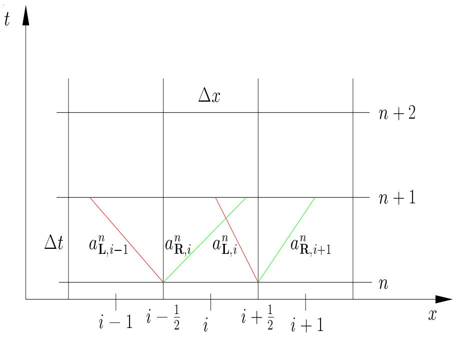

Figure 2.1: Propagation speeds

In this context, $a_{\mathrm{R},i}^n$ denotes the largest and $a_{\mathrm{L},i}^n$ the smallest propagation speed in the computational cell i, cf. Figure 2.1. It is difficult to get a good estimation of the propagation speeds. An underestimation of these values leads to spurious oscillations as the eigenvalues λ_i underestimate the physical shock wave propagation speed. Especially at condensation processes, oscillations in the numerical scheme often occured, [4, 25]. In order to avoid these numerical instabilities we set the propagation speeds in the computational cells to the so-called grid speeds $\Delta z/\Delta t$. This means that the estimated propagation speed is locally increased to the largest speed possible.

This technique is often used for processes with highly variable propagation speeds, cf. [7, 10]. The value Δt is then computed by

$$\Delta t = \lambda_{CFL} \frac{\Delta z}{\max_{k,i} \mid (\lambda_{k,i}^n \mid)}, \quad k \in \{1, 2, 3, 4\},\ i \in \{1, 2, \ldots, N\}. \tag{2.11}$$

The value λ_{CFL} denotes the so-called CFL-number. In order to guarantee stability of the numerical scheme, it has to be chosen suitably with $0 < \lambda_{CFL} \leq 1$. A CFL-number near one requires an accurate estimation of the propagation speed.

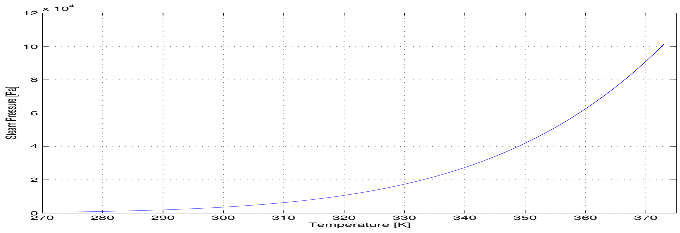

Figure 3.2: Steam pressure for water as a function of temperature

Therefore, an estimation of the propagation speed is required. In contrast to flows of ideal gases, a functional representation of the speed of sound as a function of the density and the specific total energy is not available. As a consequence we utilise the estimation

$$c^2 \approx \frac{\partial p(\rho, T)}{\partial \rho}\Big|_{T=T^n}$$

with $T^n = const$ in each time step for the propagation speed.
Finally, the ordinary differential equation

$$\mathbf{u}_t = \begin{pmatrix} \Gamma \\ -\Gamma \\ 0 \\ 0 \end{pmatrix}. \tag{2.12}$$

is solved to get a numerical solution for (2.2). Note that (2.12) has not to be solved for a flow with constant mass fraction μ.

3 Thermodynamic model for the source term

To obtain results for the system of equations (2.2) it needs to be closed. Therefore one of the unknowns must be modeled and expressed in other physical properties. In this paper, a thermodynamic equilibrium model is used. We have chosen this model, because it does not contain any additional parameters wich would be difficult to obtain such as the diameter of steam bubbles or the number of nucleis. Due to a pressure loss or a rarefaction wave [4, 14], the fluid reaches the vapor pressure $p_{\text{evap}}(T)$ and starts to evaporate. We assume the evaporation to be on a path of constant enthalpy. The maximum amount of heat, that can be received due to the evaporation process, is $\Delta h = h''(p) - h'(p)$. Therefore, the mass fraction μ can be calculated by

$$\mu(p) = \frac{h(p_{evap}(T)) - h'(p)}{h''(p) - h'(p)} \quad \text{for} \quad p_{tr} < p \leq p_{evap}(T), \tag{3.13}$$

with p_{tr} denoting the pressure at the triple point of the fluid. The presented model (3.13) does not take surface tension σ or over heating effects into account which both can be observed in real processes. The presented can be used for studies of cavitation processes and basic phenomena of two phase flows which will be described in the last section. Note, that the steam pressure p_{evap} depends on the temperature T, as shown in Figure 3.2 for the medium of water computed using the algorithms of Wagner et.al., [22].
The source term Γ used in the system (2.2) can be transformed to

$$\begin{aligned} \Gamma = \rho \frac{\mathrm{d}\mu}{\mathrm{d}t} = \rho \frac{\mathrm{d}\mu}{\mathrm{d}p}\frac{\mathrm{d}p}{\mathrm{d}t} &= -\rho \frac{1}{h'' - h'}\left[\frac{\mathrm{d}h'}{\mathrm{d}p}\Big|_{si} + \mu\left(\frac{\mathrm{d}h''}{\mathrm{d}p}\Big|_{si} - \frac{\mathrm{d}h'}{\mathrm{d}p}\Big|_{si}\right)\right]\frac{\mathrm{d}p}{\mathrm{d}t} \\ &\approx -\rho \frac{1}{h'' - h'}\frac{\mathrm{d}h'}{\mathrm{d}p}\Big|_{si} \end{aligned}.$$

This representation allows us to use the function $\mu(p,T)$ directly from (3.13). Note that we need to employ the material derivative

$$\frac{dp}{dt} = \frac{\partial p}{\partial t} + v\frac{\partial p}{\partial z}$$

as evaporation represents a process on the path. For the equation of state for the steam the ideal gas law is used, i.e. $p = \rho_G R_{H_2O} T$. The equations of Van der Waals, Benedict-Weber-Rubin, Redlich-Kwong, and Hirschfelder-Buehler-McGee-Sutton, [12, 26], could be used as well for the steam phase. For the fluid, the properties of water $\rho_L = \rho_L(p,T)$ and $e_L = e_L(p,T)$, derived by Wagner et.al. are used, cf. [22]. These functions can also be used to compute the mass fraction of steam for a given pressure $p_{tr} < p \leq p_{\text{evap}}(T)$ and temperature T, cf. [2]. For $p_{tr} < p \leq p_{evap}(T)$ the density of the fluid is fixed by a constant due to the density function of Wagner et.al. representing the mixture density ρ for this range.
The discretization of Γ in order to solve (2.12) numerically is realized in the following way

$$\Gamma_i^n = \rho_i^{n+1/2} \cdot \frac{d\mu}{dp}\Big|_i^{n+1/2} \left(\frac{p_i^{n+1/2} - p_i^n}{\Delta t} + v_i^n \frac{p_{i+1}^{n+1/2} - p_{i-1}^{n+1/2}}{2\Delta z} \right) \tag{3.14}$$

where the derivative of the mass fraction by the pressure and temperature can be derived analytically by (3.13) for the full time step Δt. On the boundaries of the computational domain the central derivative of the pressure by the space is replaced by the one-side derivatives.
We assume, that for acoustic cavitation the change of temperature is due to the high heat capacity of the fluid in a small range. Large variations of temperature are provoked by a flow through throttles where a decrease of pressure may lead to an enormous increase of temperature which can lead to a strong evaporation of the fluid. These processes are escorted by pressure waves which influence the steam-fluid mixture significantly. The presented test cases are steps to simulate these complicated physical processes.
The extension of the presented model to other fluids is theoretically quite simple. One has to measure the steam pressure p_{evap} as a function of the pressure p and temperature T. Furthermore, the evaporation enthalpy has to be measured by experiments for the fluid. The experimental determination of the mass fraction $\mu(p,T)$ is indeed very expensive and time consuming.

4 Numerical examples

For the numerical simulations we consider two different Riemann problems (cf. Figure 4.3 with left state $\mathbf{u}_L$ and right state $\mathbf{u}_R$) in a pipe with a constant cross sectional area $A = 10^{-6}\text{m}^2$ and length $l = 0.1\text{m}$, which are typical values for a pipe of an injection system. The first example deals with open ends of the pipe at the beginning of the simulation, while the left side is closed after 10^{-5} s. For the second example the ends are closed by fixed walls during the complete simulation. In all calculations we assume the pipe to be completely filled with a gas-liquid mixture, which is defined by the properties of the water-gas mixture.

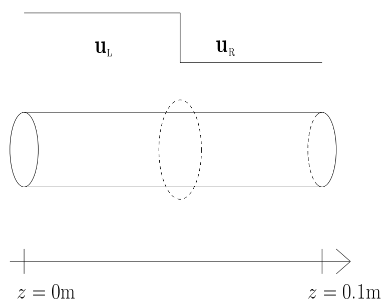

Figure 4.3: Schematic Riemann Problem

Example 1:
Table 4.1 shows the initial values for $t = 0$. The CFL number is fixed by 0.9 for the whole simulation. Δt needs to be computed in each time step again. The initial mass fraction of

	p_{left} [Pa]	v_{left} [m/s]	p_{right} [Pa]	v_{right} [m/s]	T [K]	$p_{evap}(T)$ [Pa]
1.	10^5	1	10^5	1	293.15	2300
2.	10^5	1	10^5	1	313.15	7400
3.	10^5	1	10^5	1	333.15	19900
4.	10^5	1	10^5	1	353.15	47400

Table 4.1: Initial values of the Riemann problem of example 1 for $t = 0$ s

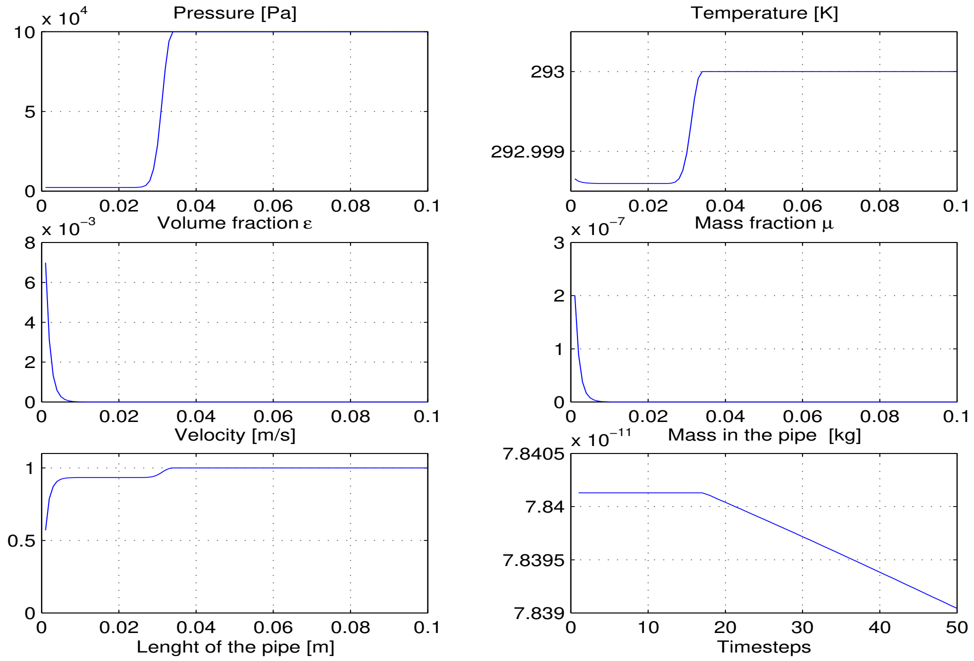

Figure 4.4: Distribution of pressure, temperature, velocity, mass fraction and volume fraction in the pipe after $30.32\mu s$ and plot of the mass in the pipe at $T = 293.15K$.

unsolved air is fixed by $\mu_0 = 10^{-8}$ which remains constant during the whole simulation. These assumptions are also valid for the second example. The results are obtained with the Fortran 90 code derived in [5]. The graphical evaluation was done with the commercial program Matlab 6.
The first case can be interpreted as follows: the gas-liquid mixture flows with constant velocity in a pipe. Suddenly, the left side of the pipe (at $z = 0$) is completely closed (the velocity at the cell face is fixed by $v = 0$) which corresponds to an infinitely fast working valve. Consequently, due to the inertia of the fluid, the pressure drops under the steam pressure, and the fluid starts to evaporate.
The Figures 4.4 - 4.7 represent the distribution of the pressure p, the temperature T, the volume fraction ε, the mass fraction μ, the velocity v, and the mass within the pipe pipe for the parameter set according to Table 4.1. In each case we show the results after 50 calculated time steps. The differences in the propagation speed due to the cavitational effects are the reason for the different total times.

With a higher temperature, the evaporated mass increases because the steam pressure depends on the temperature as shown in Figure 3.2. On the other hand, the maximum value of the volume fraction ε becomes smaller. This effect has a great meaning for experimental investigations. The volume fraction is the physical property visible in experiments. One can only draw a conclusion

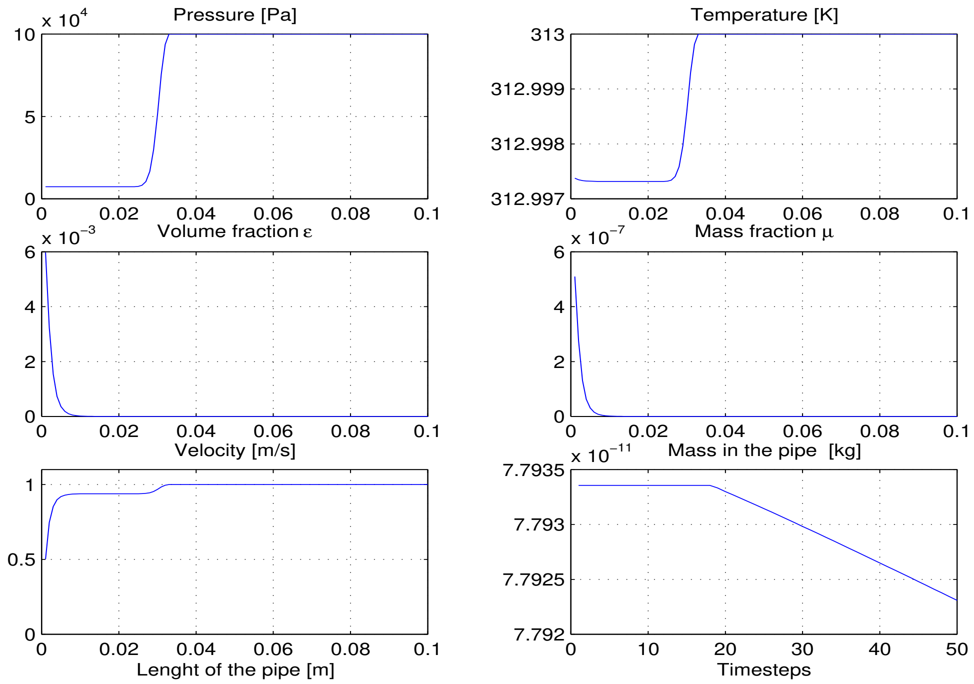

Figure 4.5: Distribution of pressure, temperature, velocity, mass fraction and volume fraction in the pipe after $29.37\mu s$ and plot of the mass in the pipe at $T = 313.15K$.

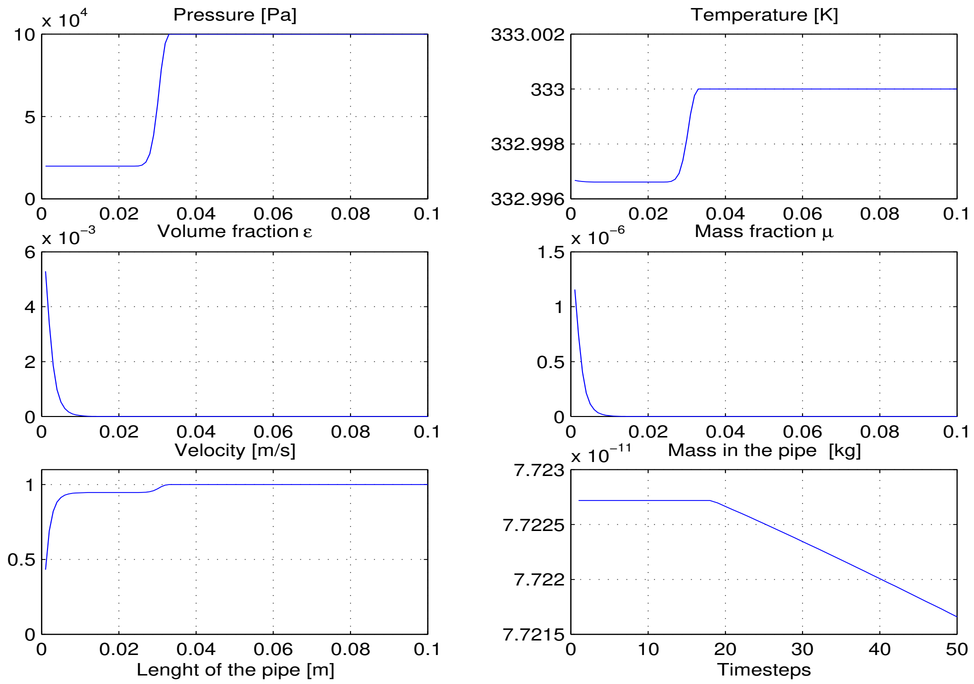

Figure 4.6: Distribution of pressure, temperature, velocity, mass fraction and volume fraction in the pipe after $28.94\mu s$ and plot of the mass in the pipe at $T = 333.15K$.

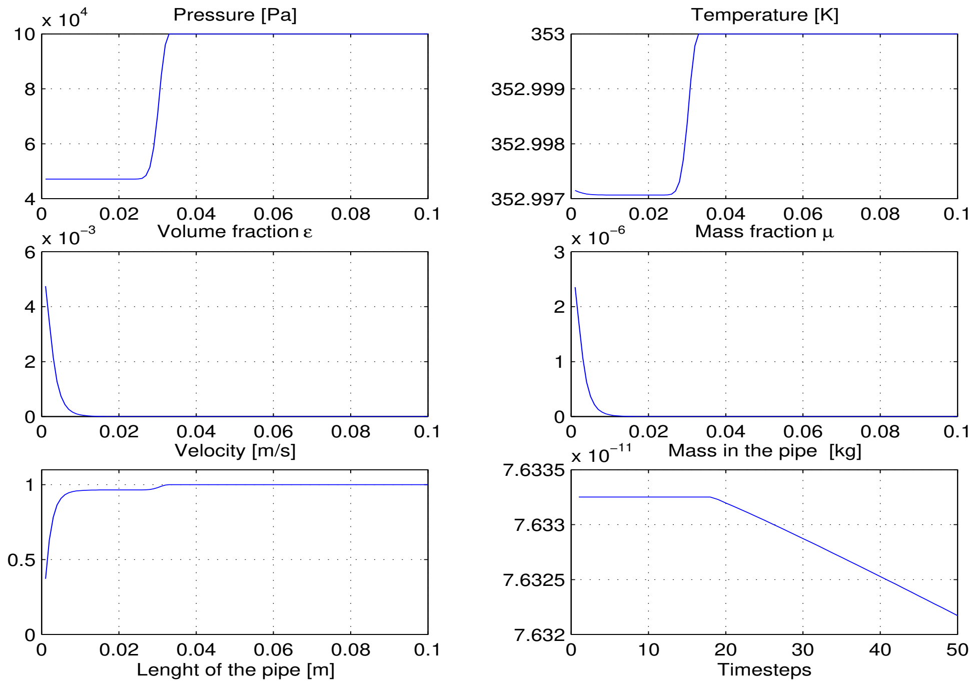

Figure 4.7: Distribution of pressure, temperature, velocity, mass fraction and volume fraction in the pipe after $28.88\mu s$ and plot of the mass in the pipe at $T = 353.15K$.

	p_{left} [Pa]	v_{left} [m/s]	p_{right} [Pa]	v_{right} [m/s]	T [K]
1.	10^7	0	10^5	0	313.15
2.	10^6	0	$7 \cdot 10^4$	0	313.15
3.	10^5	0	$5 \cdot 10^3$	0	313.15
4.	10^4	0	$5 \cdot 10^3$	0	313.15

Table 4.2: Initial data of the Riemann problem of example 2 for $t = 0$ s.

from the volume fraction ε to the mass fraction μ by the knowledge of the temperature T and the pressure p at a corresponding place. Another interesting fact is, that during evaporation pressure and temperature are nearly constant. As well-known for adiabatic flow, the temperature decreases due to a pressure loss. The high specific heat capacity leads to a very small decrease of temperature for a pressure loss of approximately $9 \cdot 10^4$ Pa.

Example 2:
The second example deals with wave motions in a pipe with 0.1m lenght and a diameter of 0.01m . In industrial applications, the wave motion in pipe systems is produced by fast opening and closing valves. The description of the fast opening valves as boundary conditions of hyperbolic systems of equations is very complicated due to the fluid-structure interaction and requires a detailed modeling which is not done here. To obtain wave motions, we consider Riemann problems with different pressure levels at the left and right side of $z = 0$ and reflecting boundaries on either side (implemented according to Toro, [21, p.210-212]). Refer to Table 4.2 for the definition of the initial values.
As mentioned above, we are interested in the simulation of the wave motion and computation of physical relevant parameters starting with different initial data. Figures 4.9-4.12 show the results after 50 calculated time steps for this second example. Again the differences in the total time

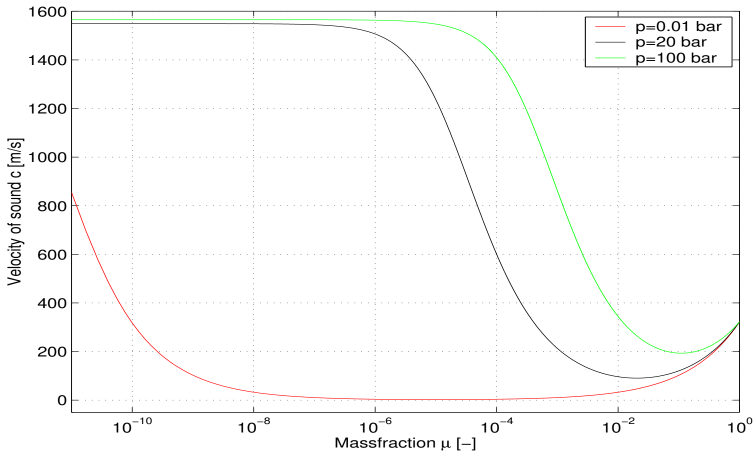

Figure 4.8: Dependence of the speed of sound c on the massfraction μ for constant pressure p and temperature T .

result from the dependence of the speed of sound on the volume fraction. The initial temperature is set constant for each problem. As shown in Figure 4.8 the speed of sound and consequently the positions of shock waves strongly depend on the mass fraction of gas/steam. Due to this, cavitated flow has to be simulated fully compressible which is done here. Figures 4.9 and 4.10 contain the graphical representation of wave motion without phase transition, while the last two simulations (refer to Figures 4.11 and 4.12) deal with condensation processes. In these two last cases, a shock wave passes a cavitation zone and due to the increase of pressure, the fluid condensates. As known, the speed of sound strongly decreases and as a result of this phenomena, the velocity is limited too. Thus, the propagation speed of the rarefaction wave is larger than the propagation speed of the shock.
As we can see in the Figures 4.9-4.12, the conservation of mass is guaranteed by the chosen numerical method. The small differences in the cavitated examples are due to the rounding errors of numerical calculations.

5 Conclusion

In this paper, a homogeneous cavitation model on the basis of mechanical and thermodynamic equilibrium is introduced. Hereby, the complete system of conservation equations consisting of mass conservation of both phases coupled by a source term, the momentum equation and the energy equation for the mixture were used. To close the system of hyperbolic equations, the thermodynamic and caloric equation of state for water were employed. The simulations of cavitated flow are connected to several difficulties, for example the large range of mixture density and the speed of sound. In connection with the described stabilization technique and the operator splitting method, cavitated flow can be simulated successfully. In contrast to [4] a continuity equation for each phase is used. This approach does not lead to any oscillations behind the shock wave in contrast to the approach using one equation for the conservation of mass.
The next step will be to model boundary conditions and to add more physical properties of the cavitation process, in particular to use more detailed source terms for the phase transition as proposed in [13, 24]. These models contain more physical parameters which can be used to study the dependence of the models and the flow equations. The developed code allows to study the overheating effects for acoustic cavitation in hot fluid flow which plays an important role in the development and simulation of gasoline injection systems.

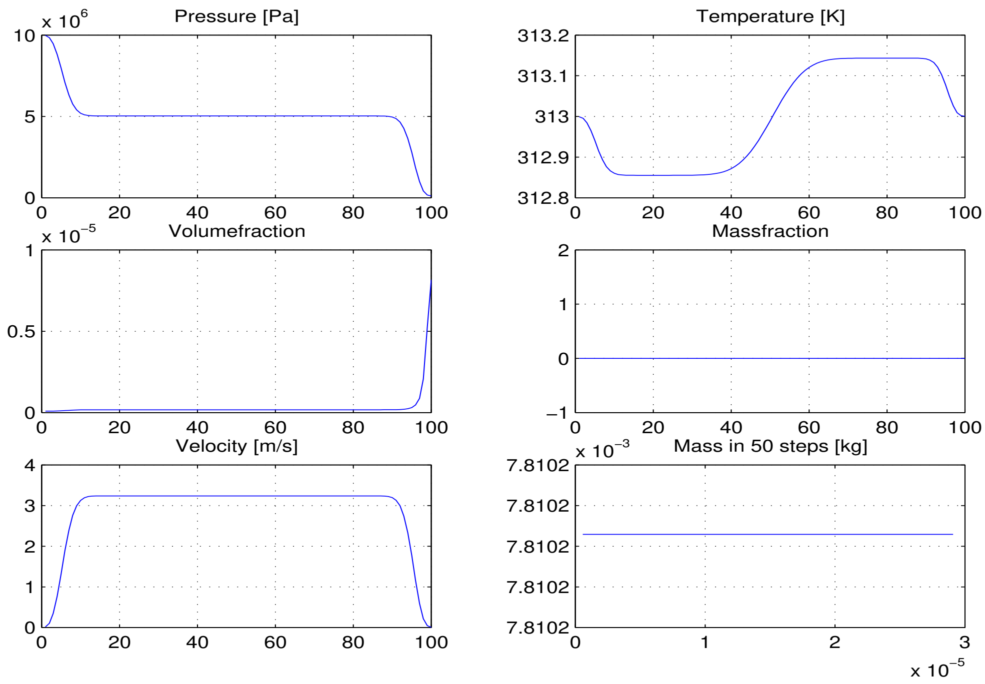

Figure 4.9: Distribution of pressure, temperature, velocity, mass fraction and volume fraction in the pipe after $29.08\mu s$ and plot of the mass in the pipe for a jump discontinuity of $p_L = 10^7 Pa$ to $p_R = 10^5 Pa$.

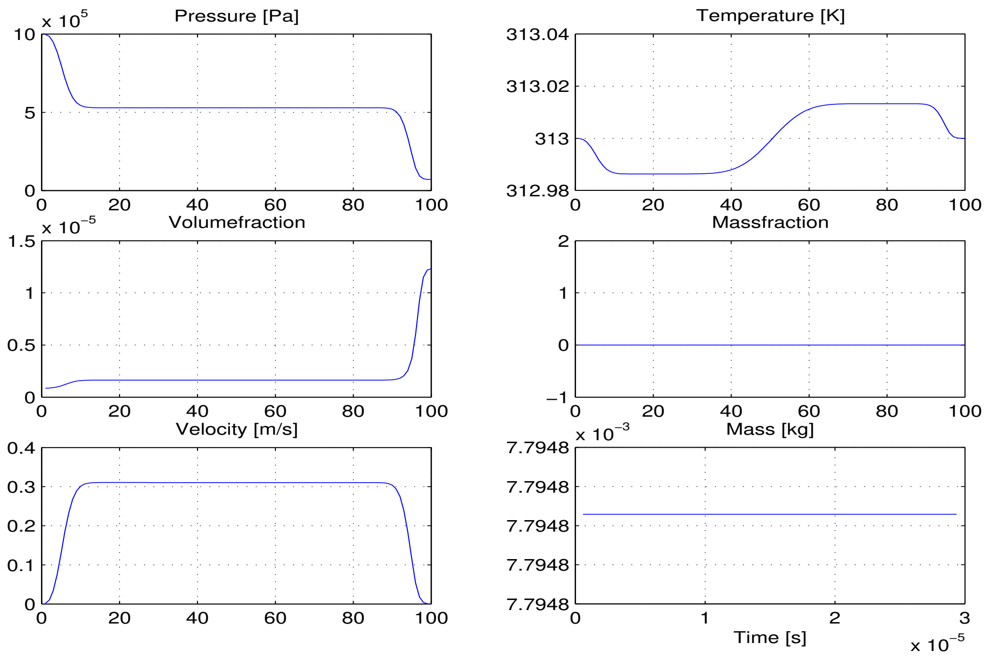

Figure 4.10: Distribution of pressure, temperature, velocity, mass fraction and volume fraction in the pipe after $29.36\mu s$ and plot of the mass in the pipe for a jump discontinuity of $p_L = 10^6 Pa$ to $p_R = 7 \cdot 10^4 Pa$.

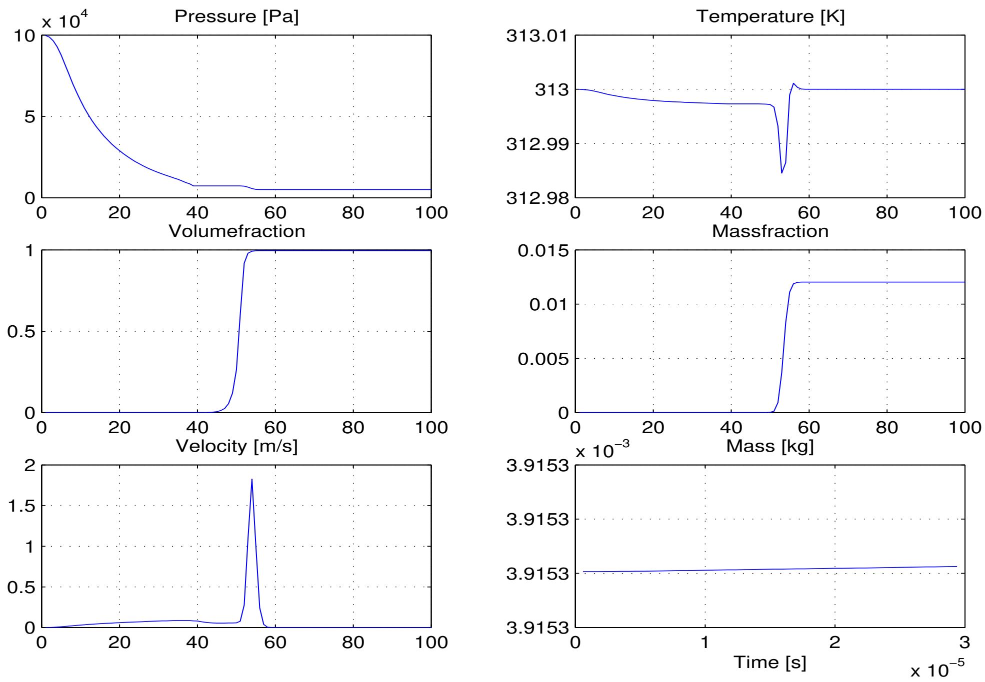

Figure 4.11: Distribution of pressure, temperature, velocity, mass fraction and volume fraction in the pipe after $29.39\mu s$ and plot of the mass in the pipe for a jump discontinuity of $p_L = 10^5 Pa$ to $p_R = 5 \cdot 10^3 Pa$.

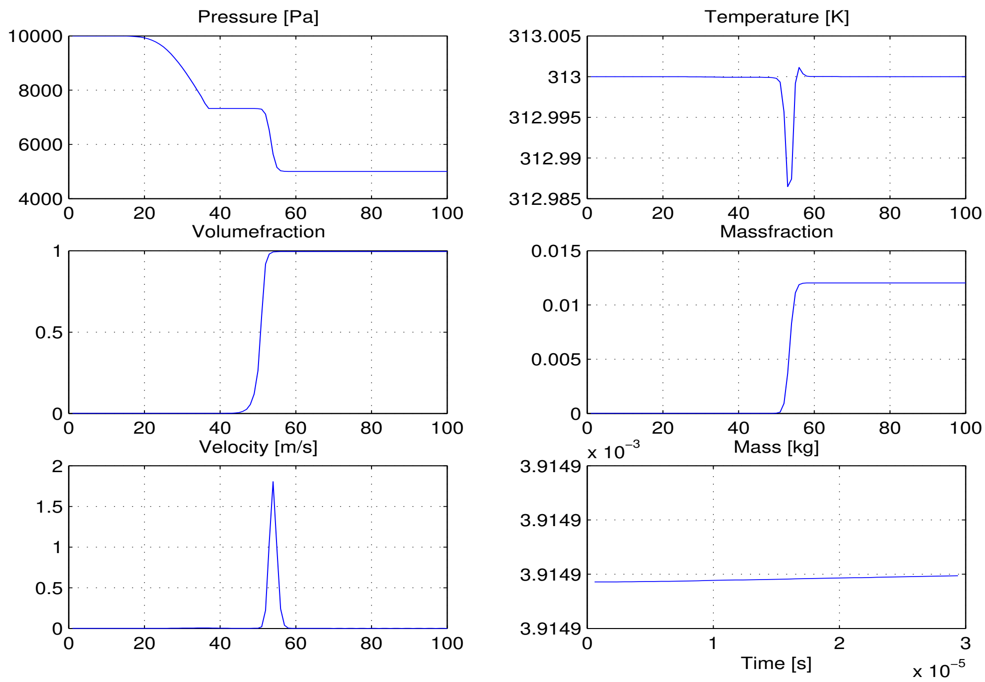

Figure 4.12: Distribution of pressure, temperature, velocity, mass fraction and volume fraction in the pipe after $29.39\mu s$ and plot of the mass in the pipe for a jump discontinuity of $p_L = 10^4 Pa$ to $p_R = 5 \cdot 10^3 Pa$.

Acknowledgment
We would like to thank our collegues F. Wrona, H. Lauterbach and K. Reymann, Dept. FV/FLM, Robert Bosch GmbH for useful discussions and hints.

References

[1] M. Athavale, Y. Jiang, and A. Singhal, *Apllication of the fuel cavitation model to pumps and inducers*, 1999. CFD Research Cooperation, Huntsville,USA.

[2] H. Baehr and K. Stephan, *Wärme- und Stoffübergang*, Springer-Verlag, 1994.

[3] T. Baur, *Auswirkungen der Diffusion glöster Gase auf das Wachstum von Kavitationsblasen*, 1997. Diplomarbeit am Institut für Wasserbau und Wasserwirtschaft.

[4] M. Beck, U. Iben, N. Mittwollen, H.-K. Iben, and C.-D. Munz, *On solution of conservation equations in cavitated hydraulic pipelines*, in 3rd International Symposium on Computational Technologies for Fluid/Thermal/Chemical Systems with Industrial Applications, 2001 ASME Pressure Vessels and Piping Conference July 22-26, Hyatt Regency, Atlanta, Georgia, USA, 2001.

[5] A. Berg, *Ein Beitrag zur numerischen Simulation von Kavitation in ein und zwei Raumdimensionen*, 2001. Diplomarbeit, Universität Hamburg.

[6] C. Brückner, *Structure and dynamics of the wake bubbles and its relevance for bubble interaction*, Physics of fluid, 11 (1999).

[7] B. Einfeldt, C.-D. Munz, P. Roe, and B. Sjögreen, *On Godunov-type methods near low densities*, J. Comput. Phys., 92 (1991), pp. 273–295.

[8] I. Hapke, *Theoretische und numerische Untersuchungen an Kavitationsmodellen*, 1995. Diplomarbeit, Universität Magdeburg, ISUT.

[9] T. Hapke and H.-K. Iben, *Modellierung und Berechnung der Kavitation in instationären Leitungsströmungen*, MTZ, 59 (1998).

[10] A. Harten, P. Lax, and B. van Leer, *On upstream differencing and Godunov-type schemes for hyperbolic conservation laws*, SIAM Rev., 25 (1983), pp. 35–62.

[11] J. Huhn and J. Wolf, *Zweiphasenströmung*, VEB Zweiphasenströmung, 1975.

[12] H.-K. Iben and J. Schmidt, *Starthilfe Thermodynamik*, Teubner Verlag, 1999.

[13] U. Iben, *Cavitation modeling*, 2000. submitted to Analysis, modelling and simulation, Gordon Breach publishing.

[14] ——, *Entwicklung und Untersuchung von Kavitationsmodellen im Zusammenhang mit transienten Leitungsströmungen*, 2001. in preparation.

[15] N. Kolev, *Transiente Zweiphasen-Strömung*, Springer-Verlag Berlin, 1986.

[16] R. T. Lahey and G. Wallis, *Non-equilibrium two-phase flows*, The American Society of Mechanical Engineers, 1975.

[17] H. Nguyen-Schaefer and H. Sprafke, *Numerical study on interaction effects of bubbles induced by air-release and cavitation in hydraulic systems*, in Tenth Bath International Fluid Power Workshop, Research Studies Press, John Wiley and Sons, 1998.

[18] C.-D. Ohl and E. Ory, *Aspherical bubble collaps - comparison with simulations*, in Nonlinear Acoustics at the Turn of the Millennium, W. Lauterborn and T. Kurz, eds., American Institute of Physics, 2000, pp. 393–396.

[19] G. Regner, *Blasendynamisches Kavitationsmodell für eine eindimensionale Strömungssimulation*, PhD thesis, Technische Universität Graz, 1999.

[20] P. Sprafke, *Numerische und experimentelle Untersuchungen des dynamischen Verhaltens hydraulischer Systeme unter Berücksichtigung von Kavitation und Luftausgasung*, PhD thesis, Universität Karlsruhe, Fakultät Maschinenbau, 1999.

[21] E. Toro, *Riemann solvers and numerical methods for fluid dynamics*, Springer Verlag, 1997.

[22] W. Wagner, S. Span, and T. Bonsen, *Wasser und Wasserdampf*, Springer Verlag, 1999.

[23] W. Wallis, *One dimensional two-phase flow*, McGraw Hill, 1975.

[24] L. v. Wijngaarden, *Hydrodynamic interaction between gas bubbles in liquid*, J. Fluid Mech., (1976), pp. 27–44.

[25] F. Wrona, *Numerische Umsetzung von homogenen Kavitationsmodellen*, Universität Stuttgart, 2001. IAG.

[26] M. Yorizane and H. Masuoka, *Equations of state at high pressure from standpoint of gas-liquid equlibria*, International Chemical Engineering, 9 (1969).